Materials Science & Engineering A 689 (2017) 89–95

Contents lists available at ScienceDirect

Materials Science & Engineering A

journal homepage: www.elsevier.com/locate/msea

Micromechanical modeling of fatigue behavior of DP steels

Ghazal Moeini[a,*], Ali Ramazani[b], Veera Sundararaghavan[b], Carsten Koenke[a]

[a] Institute for Materials Research and Testing, Bauhaus-Universität Weimar, Weimar, Coudraystraße 4, 99423, Germany
[b] Department of Aerospace Engineering, University of Michigan, 1320 Beal Ave., Ann Arbor, USA

ARTICLE INFO

Keywords:
Dual-phase steel
Dislocation density model
Kinematic hardening
Chaboche hardening model
Representative volume element

ABSTRACT

The effect of martensitic phase fraction on the cyclic stress-strain behavior of two DP steels is investigated via a micromechanical model based on a representative volume element (RVE). A dislocation density based model and a Chaboche hardening model are used to identify the isotropic and kinematic hardening behavior of constituent phases, respectively. The Chaboche parameters obtained by fitting flow curves computed from a dislocation density based model for both ferrite and martensite phases of each steel are incorporated into a Finite Element code ABAQUS to simulate the low cycle fatigue with a combined hardening behavior. Based on experimental observations reported in the literature, fatigue crack initiates in ferrite phase. A ductile damage model, therefore, is used to simulate damage initiation in ferrite. The results show that the martensite fraction has a significant influence on cyclic plastic strain accumulation during the cyclic deformation. It is also concluded that with an increase in the martensite volume fraction in DP steel, the elastic component of the total strain amplitude increases and higher fatigue strength is, subsequently, observed.

1. Introduction

Dual phase (DP) steels having a microstructure consisting of a soft ferrite matrix and metastable hard martensite result in a combination of high strength and high ductility as well as work hardening, which can all be beneficial for industrial applications [1]. High strain hardening and strong bake hardening effects give these steels excellent potential for automotive applications such as in body side, reinforcement and engine cradle [2–4]. Furthermore, these great macroscopic mechanical properties strongly depend on microstructure features such as volume fraction and morphology of martensite, ferrite grain size, geometrically necessary dislocations (GNDs) and presence of additional phases such as bainite and retained austenite [1,5,6]. In cyclic loading, all these elements must allow for high fatigue performance, which is required of DP steels along with strength and toughness.

Many engineering components are subjected to different cyclic loading conditions during engineering applications that can make them undergo cyclic plastic flow. The accumulated plastic strain in the microstructure during the cyclic loading will lead eventually to fatigue failure. On the other hand, since the fatigue life of high strength steels typically can not be enhanced as much as can the yield strength, consideration of the fatigue strength of materials during the service life becomes crucial for many applications in mechanical engineering [7]. Suresh [8] provides a comprehensive description of mechanics and micro-mechanisms of fatigue. He concluded that fatigue cracks mostly initiate from stress concentration points where the plastic deformation occurs. Intensive research has been carried out to better understand the effect of the microstructure variations on the mechanical properties of DP steels. Yang and Chen [9], in particular, studied the effect of martensite volume fraction on the mechanical properties of DP steels. Sherman and Davies [10] showed that work hardening, which is a consequence of flow-induced changes in microstructure, has a large influence on the fatigue behavior of DP steels. Ramazani et al. [11] examined the effect of martensite morphology on the failure behavior of DP steels. They showed that martensite cracking was the main failure initiation mechanism in equiaxed and banded DP steels, but that failure initiation occurred in the equiaxed microstructure at higher plastic strain than in the banded microstructure. Therefore, DP steel with equiaxed microstructure shows better failure behavior than a banded one does, although failure is initiated by the same mechanism (martensite cracking) in both microstructures. They used the extended finite element method (XFEM), in their analysis, which is appropriate when martensite cracking is the main failure initiation mechanism [11].

Hadianfard [12] reported experimentally on the effect of strain amplitude in cyclic loading and showed that at high strain amplitudes damage initiates at fractured martensite and progresses through areas with high density of martensite [12]. Mediratta et al. [13] reported that the non-uniform dislocation arrangement in coarse martensite islands encapsulated in a ferrite matrix resulted in poor low cycle fatigue life.

* Corresponding author.
E-mail address: ghazal.moeini@uni-weimar.de (G. Moeini).

http://dx.doi.org/10.1016/j.msea.2017.02.033
Received 4 November 2016; Received in revised form 28 January 2017; Accepted 8 February 2017
Available online 14 February 2017
0921-5093/

This occurs when the structures are subjected to heavy cyclic loadings that lead to induce irreversible strains on small and large scale. Paul et al. [22] showed that DP steels with fine martensite morphologies have higher fatigue life than do those with coarse martensite morphologies for all martensite volume fractions. They have reported that the fatigue cracks initiated inside the soft ferrite grains for all the samples [22].

In addition to experimental identification of the influence of microstructure on mechanical properties, recently, computational modeling has been aggressively pursued to model the material behavior at microstructure level. Nemat-Nasser et al. [14], in particular, developed a successful methodology to study the micromechanical behavior at the meso/macroscale by using a representative volume element (RVE) method. Al-Abbasi and Nemes [15] developed a micromechanical model to capture the effect of the volume fraction of martensite on strength and uniform strain in DP steels. Sun et al. [16] studied the ductile failure of DP steel using the actual microstructure recorded by SEM at various stages during the deformation process. They found that without introducing a pre-existing crack and void, ductile failure occurred due to the difference in deformation behavior between the hard martensite phase and the soft ferrite phase.

Furthermore, to determine the cyclic plastic deformation by means of micromechanics, Leblond et al. [19] introduced nonlinear kinematic hardening into the Gurson-Tvergaard-Needlemann (GTN) model. Steglich et al. [20] investigated the micromechanical modeling of cyclic plasticity incorporating damage. Their work used continuum approaches based on porous metal plasticity and continuum damage mechanics to predict the cyclic plastic response, and they applied nonlinear kinematic hardening to describe deformation under cyclic loading realistically. Recently, Paul [21] adopted a microstructure-based micromechanical modeling approach to describe the tensile and cyclic plastic deformation in DP590 steel, and thereby determined that the cyclic strain accumulation in the DP steel with inhomogeneous microstructure is the basic mode of cyclic deformation.

In the previous studies, we developed a microstructure-based model to characterize and model failure initiation in DP steels using an extended finite element method (XFEM) to simulate martensite cracking on the mesoscale combined with representative volume element (RVE) modeling during monotonic loading [17,18,34]. We developed empirical equations for XFEM parameters as functions of local carbon content in martensite and showed that the equations could predict successfully failure initiation in industrially produced DP steels with various chemistries, strengths and martensite fractions [36]. Additionally, we utilized first principle calculations to calculate cohesive zone model parameters for ferrite-martensite interface decohision in DP steels as a function of martensite carbon content [37]. Implementing XFEM to martensite and cohesive zoned model to ferrite-martensite interface using identified parameters from [36,37], respectively, will help to predict failure initiation mechanism as well as failure initiation corresponding stress/strain in DP steels with various chemistries, strengths and morphologies [38]. Following our previous studies on the micromechanical modeling of failure initiation in DP steel during monotonic loading conditions, we present a micromechanical-based model to predict failure initiation of DP steels during cyclic loading conditions. For this purpose, micromechanical modeling is applied to predict the behavior of DP steel with different martensite fractions during the cyclic loading and the results are validated by comparison with the experimental observation in Paul et al. [22]. Real images of the microstructure are used to create representative volume elements subjected to cyclic loadings. The micromechanical approach associated with combined hardening model is applied to simulate the hysteresis curves of DP steel with different martensite fractions. It should be also mentioned that the ductile damage curve is used as a failure criterion for the ferrite phase for better prediction of cyclic behavior of DP steel.

Table 1
The chemical composition of the investigated steels (wt%) [22].

	C	Si	Mn	P	Cr	Al
DP Steel	0.093	0.88	1.42	0.014	0.022	0.034

Table 2
Characterization of the studied DP steels [22].

Material	Martensite volume fraction %	Ferrite grain size (μm)	Martensite grain size (μm)
DP-1	20 ± 3	8.0 ± 1.2	5.4 ± 1.1
DP-2	55 ± 5	8.6 ± 1.2	11.5 ± 1.5

2. Literature data

Paul et al. [22] investigated the effect of martensite morphology on low cycle fatigue performance of dual phase steels. The thickness of DP steel in their study was 2 mm. The chemical composition of the material is given in Table 1.

By using different heat treatment processes, they generated two DP steels with different martensite fractions and ferrite grain sizes, as summarized in Table 2. The optical micrographs of the microstructures of these DP steels [22] are shown in Fig. 1. The fully reversed (R=−1) total strain amplitude control was done. Fatigue tests were carried out at constant strain rate of 0.02 s^{-1}.

3. Numerical approach (Micromechanical modeling)

Micromechanical modeling using numerical tensile test of a representative volume element (RVE) is an appropriate procedure to study and model the flow behavior of DP steels. This method is advantageous since it provides a good description of the deformation of the material on the micro level giving insight into the stress and strain evolution and distribution in and between the phases.

An RVE has to be constructed in such a way that the shape, morphology, size and randomness of constituent phases can be considered to be representative of the microstructure under consideration. Hence, it should be sufficiently large to include the microstructural characteristics but also adequately small to optimize time expenditure for calculation. Besides the optimal size, four basic features have to be discussed to define a micromechanical model for multiphase material:

(a) Geometric definition of a representative volume element (RVE), which represents the vital features of the microstructure. Here, 2D RVE will be presented in detail in the following Section 3.1.
(b) Constitutive description of the flow behavior of each phase, which is formulated based on dislocation density theory. Furthermore, the kinematic hardening parameters of single phase will be identified based on the flow curve of each phase. Mechanical properties of single phases and the kinematic hardening parameters identification will be discussed in Sections 3.2 and 3.3, respectively.
(c) Boundary conditions imposing the loading from macroscale. In this study, periodic boundary conditions were employed on the meshed RVEs through a developed FORTRAN program to simulate the material behavior under strain controlled cyclic loading. In this approach the displacement at only four corner nodes have to be prescribed for explaining the deformation of the whole RVE which will be presented in detail in Section 3.4.
(d) Homogenization strategy needed to represent the macroscopic mechanical behavior from the results of the RVE's numerical evaluation. A computational first-order homogenization by volume

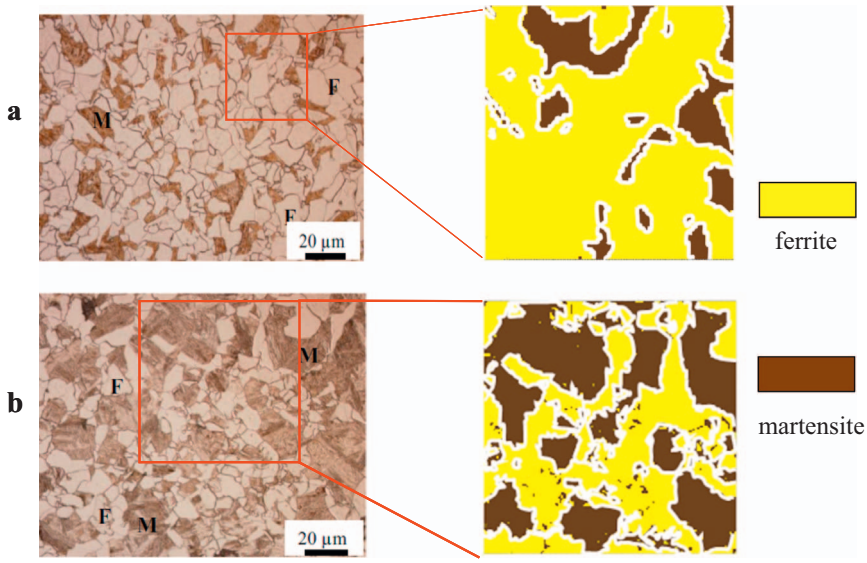

Fig. 1. RVEs from the experimental microstructure [22] a) DP-1 (V_m=20%), b) DP-2 (V_m=55%). V_m is the volume fraction of martensite On the left, the light areas are ferrite, marked "F" and the dark areas are martensite, marked "M".

averaging was applied to obtain the macroscopic mechanical behavior from the results of the RVE calculation, which will be discussed in Section 3.5.

3.1. RVE generation

A 2D representative volume element (RVE), which is intended to be representative of the entire sample, was first created from the microstructures of both studied DP steels. Selected areas of light optical microscopy (LOM) images of the experimental microstructure were converted into a 2D RVE, taking advantage of the color difference between martensite and ferrite, using an in-house finite element generator, Gitter [23]. The smallest satisfactory dimension of the RVE in DP steels is 24×24 μm^2, which should contain a minimum of 19 martensite particles, as reported by Ramazani et al. [23]. The RVE size therefore was taken to be 40 μm ×40 μm for both DP steels with 20% and 55% martensite volume fractions, respectively. Plane stress elements (CPS4R) were employed for the numerical tensile tests. Additionally, the effect of mesh size was studied by Ramazani et al. [24] with ranging element length from 0.1 to 2 μm, and no deviation was obtained for the meshes finer than 0.25 μm. Therefore, in the current study, quadratic meshes with element size of 0.25 μm were used for the modeling.

3.2. Modeling the isotropic hardening behavior of ferrite and martensite

In the current work, the elastic modulus for ferrite and martensite is assumed to be 210 GPa [24]. A dislocation-based strain-hardening model of Rodriguez and Gutierrez [25] is applied to define the flow curve of individual phases for ferrite and martensite (Eq. (1)). This model emerges from the classical dislocation theory of [26,27] and from the work of [28] and is given below.

$$\sigma\,(\text{in MPa}) = \sigma_0 + \Delta\sigma + \alpha^{*}M^{*}\mu^{*}\sqrt{b}^{*}\sqrt{\frac{1-exp\,(-MK_r\varepsilon)}{K_r^{*}L}} \quad (1)$$

Here σ and ε are the flow stress (von Mises stress) and true strain (equivalent plastic strain), respectively. The first term σ_0 describes the effect of the Peierls stress and of the alloying elements in the solid solution [25], as follows:

$$\sigma_0(\text{in MPa}) = 77 + 750(\%P) + 60(\%Si) + 80(\%Cu) + 45(\%Ni) + 60(\%Cr) + 80(\%Mn) + 11(\%Mo) + 5000(\%N_{ss}) \quad (2)$$

The second term in Eq. (1) accounts for strengthening by carbon in solution, which for ferrite is:

$$\Delta\sigma\,(\text{in MPa}) = 5000^{*}(\%C_{ss}^{f}) \quad (3)$$

and in the case of martensite is:

$$\Delta\sigma\,(\text{in MPa}) = 3065^{*}(\%C_{ss}^{m})-161 \quad (4)$$

The third term accounts for strengthening by dislocation density, precipitation hardening, grain size as well as work softening due to recovery. According to Ref. [5,29], α is a constant with a value of 0.33. M is the Taylor factor with a value of 3. μ is the shear modulus with a value of 80,000 MPa. b is the Burger's vector (2.5×10^{-10} m). k_r is the recovery rate and in the case of ferrite a value of $10^{-5}/d_\alpha$ is assumed, where d_α refers to the ferrite grain size. For martensite, the k_r value is 41. L is the dislocation mean free path. For ferrite it is the same as the grain size (d_α), while for martensite it is a constant with a value of 3.8×10^{-8} m [5,29].

The carbon content of ferrite (C_α) was approximated using ThermoCalc software with the TCFe6 database. The following elements were taken into account for ThermoCalc calculations: Mn, C, Si and Cr. The carbon content of the martensite (C_m) was calculated by considering the carbon mass balance and based on the following relation (Eq. (5)):

$$C_{DP} = C_\alpha V_\alpha + C_m V_m \quad (5)$$

where V_α, and V_m, are ferrite and martensite volume fractions, measured experimentally based on the ASTM-E562 standard [30], respectively. C_{DP} stands for the nominal carbon composition of the DP steel, determined experimentally by Paul et al. [22].

3.3. Kinematic hardening parameters identification

Because of the intense deformation incompatibilities between soft ferrite and hard martensite in DP steel, kinematic hardening has to be considered properly to obtain a good evaluation of the effect of cyclic deformation. Therefore, for micromechanical modeling of DP steel subjected to cyclic loading, the kinematic hardening models of each constituent phase should be determined. In the current study, the kinematic hardening behavior introduced by Chaboche [31] is used for ferrite and martensite, expressed as:

$$d\bar{\alpha} = \sum_{i=1}^{3} d\alpha_i \tag{6}$$

$$d\bar{\alpha}_i = \frac{2}{3}.\ C_i.\ d\bar{\varepsilon}_{PL} - \gamma_i \bar{\alpha}_i d\varepsilon_p \tag{7}$$

Here, $d\bar{\varepsilon}_{PL}$ and $d\varepsilon_p$ denote the plastic strain increment vector and equivalent plastic strain increment, respectively. C_i and γ_i are Chabche material constants. In the third order Chaboche model, the index i denotes the individual back-stress tensor, ranging from 1 to 3. The first term in Eq. (7) represents the hardening modulus and the second term is a "recall term" that exhibits the nonlinear effect. The material constant γ_i controls the hardening rate during the plastic deformation. The total back stress is a summation of three back stresses ($\alpha = \alpha_1+\alpha_2+\alpha_3$). In which the first back stress (α_1) present the high plasticity modulus at the yielding point which saturates rapidly. (α_2) present the nonlinear part of the hysteresis curve and the last back stress ((α_3) simulate the linear hardening at higher strain range. The loading part of flow curve is represented as:

$$\sigma = \sigma_0 + \alpha_1 + \alpha_2 + \alpha_3 \tag{8}$$

where σ_0 is initial yield stress. Although Chaboche suggested estimating the material constants from the stabilized hysteresis curve, Gilman et al. [32], Ohno and Wang [33] and Zhang and jiang [34] determine the parameters of the Chaboche model based on monotonic stress-strain curve. Additionally, they introduced a nonlinear kinematic hardening material model of Chaboche for elastic-plastic ratcheting analysis. In the current study, we utilize the flow curve of ferrite and martensite from a dislocation density based model, as discussed in Section 3.2, to identify the Chaboche model parameters The value of C1 is determined from the slope of stress-strain curve at the yield point. The value of γ_1 should be large enough that α_1 saturates rapidly. C_3 can be determined as a constant slope of stress-strain curve at a high strain rage. Also, the value of C_2 and γ_2 proposed by trial and error in order to satisfy the Eq. (8).

Since Paul et al. [22] showed failure initiation occurred in ferrite during the low cycle fatigue, we utilized the ductile damage curve to simulate ferrite degradation [35] in our micromechanical modeling of DP steel during cyclic loading. The ferrite damage curve, derived in [35], is based on the stress triaxiality and equivalent plastic strain that represents the critical local stress strain response for ductile crack initiation (Eq. (9)). Where ε_e^{pl} and η are the equivalent plastic strain and stress triaxiality, respectively.

$$\varepsilon_e^{pl} = 0.\ 239 \times e^{-1.678 \times \eta} + 0.\ 107 \tag{9}$$

Finite element simulation was carried out using the ABAQUS standard code to predict the cyclic behavior of RVEs during the uniaxial stain controlled cyclic loading. The strain amplitude and constant strain rate were taken to be 0.5% and 0.02 s^{-1} respectively, which were equal to those used in the experiments.

3.4. Periodic boundary conditions (PBCs)

As the RVE is just a small part of the total tensile test specimen, periodic boundary condition can be imposed on the RVE. An advantage of using periodic boundary conditions is that the displacements at only four corner-nodes have to be prescribed to describe the deformation of the whole RVE. Furthermore, it gives a better estimation of the overall properties, than other types of boundary conditions listed before. In Fig. 2a schematic representation of a 2D RVE is given with the corner nodes indicated. The boundary in this case is split into four parts, as can be seen in Fig. 2.

The Top and Bottom nodes have same displacements, while the Right and Left node have same displacements. This was done by writing equations. First the face nodes are considered in the undeformed state. For an initially periodic geometry the position vectors of

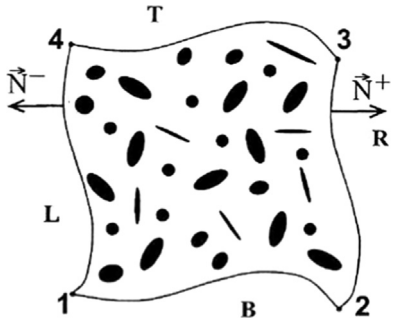

Fig. 2. Schematic representation of a 2D RVE [39].

the face-nodes are linked to the position of the corner-nodes. Therefore, the periodic boundary condition can be rewritten as (Eq. (10)) [39]:

$$\begin{aligned} \overrightarrow{X_T} &= \overrightarrow{X_B} + \overrightarrow{X_4} - \overrightarrow{X_1} \\ \overrightarrow{X_R} &= \overrightarrow{X_L} + \overrightarrow{X_2} - \overrightarrow{X_1} \\ \overrightarrow{X_3} &= \overrightarrow{X_2} + \overrightarrow{X_4} - \overrightarrow{X_1} \end{aligned} \tag{10}$$

Finally these position vectors are written in terms of displacements and then implemented in a FEM package.

3.5. Homogenization strategy

Homogenization strategy was performed to make a coupling between the macro and micro scales. In this phase of solution, the macroscopic stress components are computed as the volume average of the microscopic components according to the following equations:

$$S_{ij} = \frac{1}{V_0} \int_{V_0} \sigma_{ij} dV \tag{11}$$

$$E_{ij} = \frac{1}{V_0} \int_{V_0} \varepsilon_{ij} dV \tag{12}$$

where S_{ij} and E_{ij} are the macroscopic average component of stresses and strains over the microscopic volume of the micromechanical model [39].

4. Results and discussion

Rodriguez's approach [25], as discussed in Section 3.2, is used to develop the flow curve of ferrite and martensite for each of the two DP steels studies here. As shown in Fig. 3, the disparities between the ferrite flow curves for DP-1 and DP-2 steels are marginal, while for the martensitic flow curves the dissimilarities are considerably greater. According to our previous work [24], the increase of the strength of the martensite flow curve of DP-1 relative to DP-2 steel is primarily due to the fact that the martensite carbon content in DP-1 steels is higher than that in DP-2 steel. In ref. [24], we showed the relationship between martensite carbon content and volume percent of martensite using Thermocalc calculations. According to our results in [24], the carbon concentration of martensite decreases with increasing the volume percent of martensite in DP steels. Since there is a direct relationship between martensite carbon content and martensite yield strength (see Eq. (4) in Section 3.2), the strength of martensite in DP steel with 55% martensite will be less that the strength of martensite in DP steel with 20% martensite. In the DP steel with lower martensite fraction, the carbon content in martensite is higher based on the mass balance rule. Therefore, the strength of the martensite phase in DP-1 steel with 20% martensite is higher than in DP-2 steel with 55% martensite.

Chaboche material parameters were estimated according to the calibration process, which is well explained in [32]. According to Gilman et al. [32], the Chaboche kinematic hardening parameters are

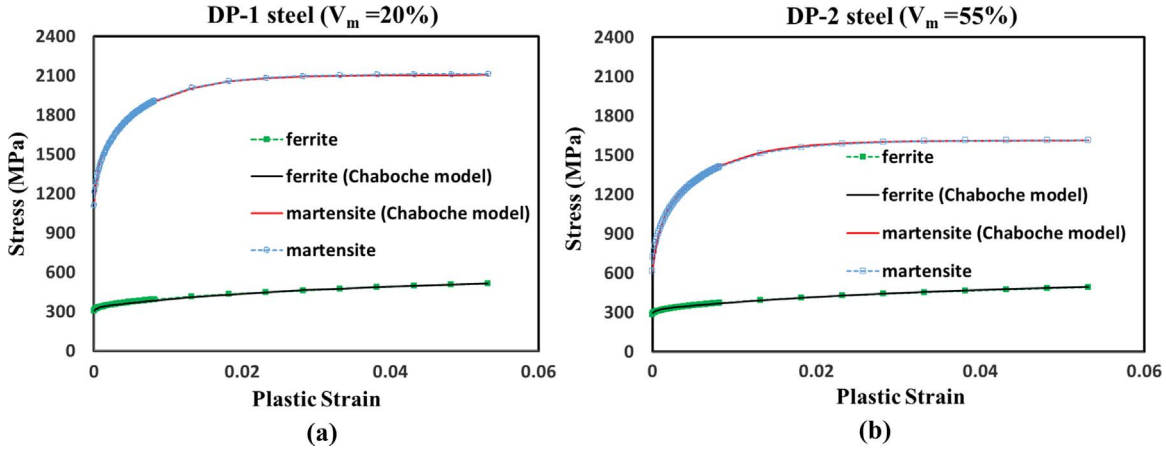

Fig. 3. Estimation of Chaboche parameters based on ferrite and martensite flow curves of (a) DP-1 steel with 20% martensite and (b) DP-2 steel with 55% martensite.

Table 3
Chaboche kinematic hardening parameters.

Material	C_1 (MPa)	C_2 (MPa)	C_3 (MPa)	γ_1	γ_2	γ_3
ferrite (steel C_20%)	45,000	6400	1000	1800	44	1.5
ferrite (steel C_55%)	42,880	5505	980	1600	39	1.5
martensite (steel C_20%)	568,000	89,600	20	1600	140	0.5
martensite (steel C_55%)	414,000	97,500	20	1200	150	0.5

identified by fitting Eq. (8) to the calculated flow curves of ferrite and martensite from Eq. (1), as illustrated in Fig. 3. The obtained Chaboche kinematic hardening parameters are listed in Table 3.

The Chaboche parameters obtained by fitting were employed to simulate the low cycle fatigue with a non-linear kinematic hardening behavior. A fully reversed strain-controlled low cycle fatigue simulation was conducted on two RVEs with different martensite volume fractions. The strain amplitude and constant strain rate were taken to be 0.5% and 0.02 s^{-1} respectively, which were equal to those used in the experiments.

During cyclic loading, strain cycling causes a rearrangement of dislocations for martensite, which leads to less resistance to deformation and then the material shows cyclic softening behavior. On the other hand, for ferrite, the dislocation density increases due to cyclic plastic straining and leads to cyclic strain hardening [12]. Therefore, strain partitioning occurs for dual-phase microstructures due to the differing flow characteristic of the constituent phases during low cycle fatigue. As shown in Fig. 4, the stress concentration in ferrite is higher than in martensite due to the cyclic hardening behavior of ferrite during cyclic loading. Also in the DP steel with the higher martensite fraction, namely DP-2 steel, the stress concentration in the martensite is significantly lower due to its lower carbon content.

The equivalent plastic strain distribution of both DP steels with 20% and 55% martensite fractions after 100 cycles is illustrated in Fig. 5. During cyclic straining, hard martensite particles resist plastic deformation in the soft ferrite which lead to inhomogeneous deformation. It can be seen that the microscale inhomogeneous deformation develops high stress concentration at the ferrite/martensite interface. In both DP-1 and DP-2 steels, formation of shear bands in soft ferrite is noticed in the RVEs after 100 cycles.

Martensite has a high yield stress and higher resistance to the plastic deformation and it is known that to activate the dislocation sources in hard martensite phase high stress required. Therefore, in this study with low strain amplitude, the accumulated plastic fatigue strain occurs mostly in the ferrite phase and sharp shear bands appear. This is also confirmed by experimental data in [12,22]. The shear bands of the localized plastic strain in the ferrite are most likely exaggerated due to the plane strain condition. The direction of the localized plastic deformation is on average 45° to the loading direction.

The hysteresis loops for the initial and 100th cycle of straining at 0.5% strain amplitude for DP-1 and DP-2 steels are given in Fig. 6. Both DP steels with different martensite volume fractions show softening behavior under low cycle fatigue. The amount of softening behavior, which indicates a decrease in resistance to the deformation, is higher in DP-1 steel with the lower martensite volume fraction than

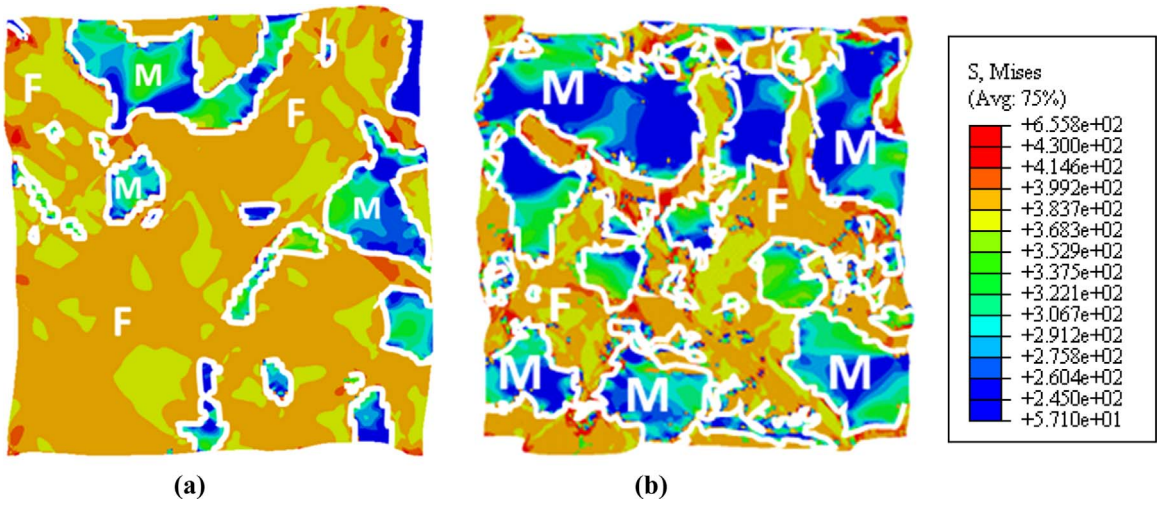

Fig. 4. Von-Mises stress distribution in (a) DP-1 steel (V_m=20%), and (b) DP-2 steel (V_m=55%) after 100 tension-compression cycles.

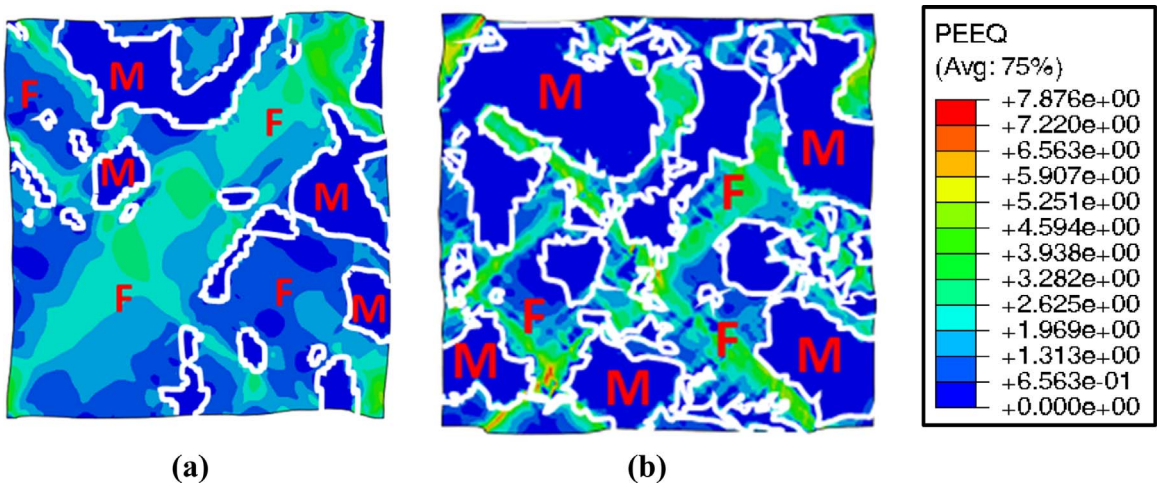

Fig. 5. Equivalent plastic strain accumulation DP-1 steel (V_m=20%), and (b) DP-2 steel (V_m=55%) after 100 tension-compression cycles (strain amplitude of 0.5%).

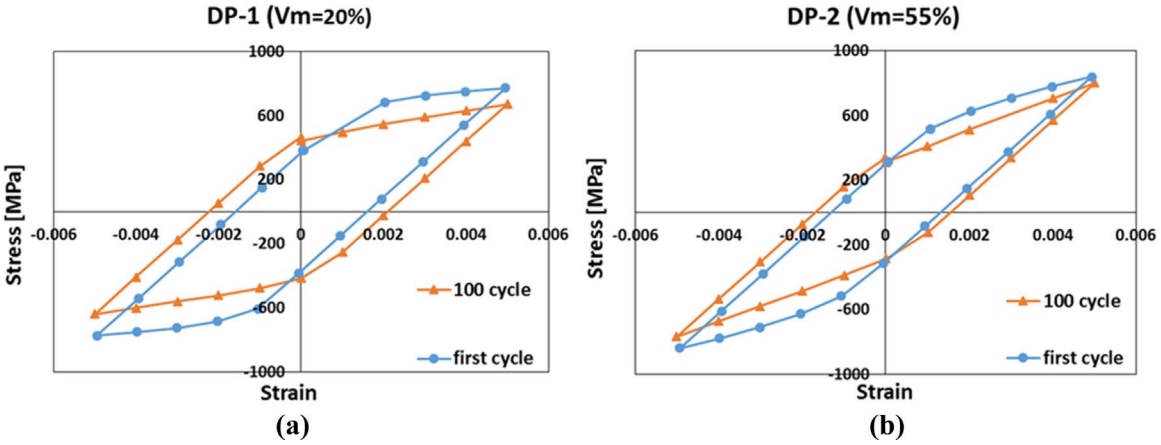

Fig. 6. Hysteresis loop under cyclic straining at a constant strain amplitude of 0.5% along the loading direction.

in the DP-2 steel with the higher martensite volume fraction. It can be seen that in the case of the high martensite volume fraction, the elastic component of the total strain amplitude is higher and therefore the fatigue strength is higher.

5. Conclusions

- For dual-phase microstructures, strain accumulation occurs in soft ferrite due to the strain partitioning. The stress concentration in ferrite is higher than in martensite due to the cyclic hardening behavior of ferrite during cyclic loading. the
- Simulation results show the cyclic softening behavior for both DP steels with 20% and 55% martensite fractions.
- Cyclic softening behavior of DP steel depends significantly on the percentage of martensite volume fraction. By increasing the martensite volume fraction, the elastic component of total strain amplitude in DP steel increases and a higher fatigue strength is, therefore, predicted.

Acknowledgment

The financial support of Bauhaus-Universität Weimar in the framework of Thüringer Graduiertenförderung is highly acknowledged.

References

[1] A. Ramazani, K. Mukherjee, A. Schwedt, P. Goravanchi, U. Prahl, W. Bleck, Int. J. Plast. 43 (2013) 128–152.
[2] T. Senuma, ISIJ Int. 41 (2001) 520–532.
[3] A. Ramazani, B. Berme, U. Prahl, Structural materials and processes in, in: D. Lehmhus, M. Busse, A.S. Herrmann, K. Kayvantash (Eds.), Transportation, Wiley-VCH, Weinheim, Germany, 2013, pp. 5–48.
[4] World Auto steel, Ultra light Steel Auto Body-Advanced Vehicle Technology, 2002. (www.Elsab.org).
[5] A. Ramazani, K. Mukherjee, U. Prahl, W. Bleck, Metall. Mater. Trans. A 43 (2012) 3850–3869.
[6] A. Ramazani, Y. Chang, U. Prahl, Adv. Eng. Mater. 16 (2014) 1370–1380.
[7] Y. Murakami, Metal Fatigue: Effects of Small Defects and Nonmetallic Inclusions, Elsevier, Oxford, Boston, 2002.
[8] S. Suresh, Fatigue of Materials, second ed., University Press, Cambridge, 2002.
[9] J.R. Yang, L.J. Chen, J. Mater. Sci. 26 (1991) 889–898.
[10] A.M. Sherman, R.G. Davies, Met. Trans. A 10 (1979) 929–933.
[11] A. Ramazani, Z. Ebrahimi, U. Prahl, Comput. Mater. Sci. 87 (2014) 241–247.
[12] M.J. Hadianfard, Mater. Sci. Eng. A 499 (2009) 493–499.
[13] S.R. Mediratta, V. Ramaswamy, P. Rama Rao, Int. J. Fatigue 7 (1985) 107–115.
[14] S. Nemat-Nasser, M. Hori, Micromechanics: Overall Properties of Heterogeneous Materials, Elsevier, Amsterdam, 1993.
[15] F.M. Al-Abbasi, Ja Nemes, Int. J. Solids Struct. 40 (2003) 3379–3391.
[16] X. Sun, K.S. Choi, W.N. Liu, M.A. Khaleel, Int. J. Plast. 25 (2009) 1888–1909.
[17] A. Ramazani, A. Schwedt, A. Aretz, U. Prahl, W. Bleck, Comput. Mater. Sci. 75 (2013) 35–44.
[18] A. Ramazani, A. Schwedt, A. Aretz, U. Prahl, Key Eng. Mater. 586 (2014) 67–71.
[19] J. Leblond, G. Perrin, J. Devaux, Eur. J. Mech. A/Solids 14 (1995) 499–527.
[20] D. Steglich, A. Pirondi, N. Bonora, W. Brocks, Int. J. Solids Struct. 42 (2005) 337–351.
[21] S.K. Paul, Model. Simul. Mater. Sci. Eng. 21 (2013) 55001.
[22] S.K. Paul, N. Stanford, T. Hilditch, Mater. Sci. Eng. A 644 (2015) 53–60.
[23] A. Ramazani, K. Mukherjee, U. Prahl, W. Bleck, Comput. Mater. Sci. 52 (2012) 46–54.
[24] A. Ramazani, K. Mukherjee, H. Quade, U. Prahl, W. Bleck, Mater. Sci. Eng. A 550 (2013) 129–139.
[25] R.M. Rodriguez, I. Gutierrez, Mater. Sci. Forum 426–432 (2003) 4525–4530.
[26] Y. Bergström, Mater. Sci. Eng. 5 (4) (1970) 193–200.
[27] Y. Estrin, H. Mecking, Acta Metall. 32 (1) (1984) 57–70.
[28] J.G. Sevillano, Mater. Sci. Technol. 6 (1993).

[29] A. Ramazani, K. Mukherjee, A. Abdurakhmanov, U. Prahl, M. Schleser, U. Reisgen, W. Bleck, Mater. Sci. Eng. A 589 (2014) 1–14.
[30] ASTM E562-11, Standard Test Method for Determining Volume Fraction by Systematic Manual Point Count, in: ASTM E562, ASTM International, 2013.
[31] J.L. Chaboche, Int. J. Plast. 7 (1991) 661–678.
[32] T. Gilman, B. Weitze, J. Rudolph, A. Willuweit, A. Kalnins, ASME 2015 Pressure Vessels & Piping Conference, Vol. 137, 2015, pp. 1–10.
[33] N. Ohno, J. Wang, Int. J. Plast. 9 (1993) 375–390.
[34] J. Zhang, Y. Jiang, Int. J. Plast. 24 (2008) 1890–1915.
[35] N. Vajragupta, V. Uthaisangsuk, B. Schmaling, S. Munstermann, A. Hartmaier, W. Bleck, Comput. Mater. Sci. 54 (2012) 271–279.
[36] A. Ramazani, M. Abbasi, S. Kazemiabnavi, S. Schmauder, R. Larson, U. Prahl, Mater. Sci. Eng. A 660 (2016) 181–194.
[37] A. Ramazani, S. Kazemiabnavi, R. Larson, Acta Mater. 116 (2016) 231–237.
[38] A. Ramazani, (Ph.D. thesis), RWTH-Aachen University, 2013.
[39] V. Kouznetsova, (Ph.D. thesis), Technical University of Eindhoven, 2002.